Cell, Vol. 96, 79–88, January 8, 1999, Copyright ©1999 by Cell Press

High-Resolution Model of the Microtubule

Eva Nogales,*†§ Michael Whittaker,‡ Ronald A. Milligan,‡ and Kenneth H. Downing*
*Lawrence Berkeley National Laboratory
Berkeley, California 94720
†Molecular and Cell Biology Department
University of California at Berkeley
Berkeley, California 94720
‡Department of Cell Biology
The Scripps Research Institute
La Jolla, California 92037

Summary

A high-resolution model of the microtubule has been obtained by docking the crystal structure of tubulin into a 20 Å map of the microtubule. The excellent fit indicates the similarity of the tubulin conformation in both polymers and defines the orientation of the tubulin structure within the microtubule. Long C-terminal helices form the crest on the outside of the protofilament, while long loops define the microtubule lumen. The exchangeable nucleotide in β-tubulin is exposed at the plus end of the microtubule, while the proposed catalytic residue in α-tubulin is exposed at the minus end. Extensive longitudinal interfaces between monomers have polar and hydrophobic components. At the lateral contacts, a nucleotide-sensitive helix interacts with a loop that contributes to the binding site of taxol in β-tubulin.

Introduction

Microtubules are ubiquitous cytoskeletal elements built by the self-association of αβ-tubulin dimers. The polymerization process involves two types of contacts between tubulin subunits: head-to-tail binding of dimers results in protofilaments that run along the length of the microtubule, and lateral interactions between parallel protofilaments complete the microtubule wall. Adjacent protofilaments are offset axially, resulting in a helical lattice of monomers that is occasionally interrupted by a "seam" where the lateral interface between protofilaments involves heterologous contacts (α-β) between monomers. The longitudinal contacts along protofilaments appear to be much stronger than those between adjacent protofilaments, based both on the fact that depolymerization involves the peeling of protofilament fragments from the microtubule ends (Mandelkow et al., 1991) and on the recurrence of the protofilament structure in all characterized tubulin polymer forms, for example rings, spirals, sheets, or ribbons. Only in microtubules and zinc-induced sheets are the protofilaments straight. In contrast with the microtubule, the zinc sheets are formed by the antiparallel association of protofilaments (Amos and Baker, 1979).

§To whom correspondence should be addressed (e-mail: enogales@lbl.gov).

We recently obtained the structure of the tubulin dimer by electron crystallography of zinc-induced tubulin sheets (Nogales et al., 1998a). Each tubulin monomer (Figure 1A) is a compact ellipsoid of approximate dimensions 46 × 40 × 65 Å (width, height, and depth, respectively) made up of three sequential domains: an N-terminal, nucleotide-binding domain; a smaller second domain; and a predominantly helical C-terminal region. The α and β subunits are very similar, with the αβ-dimer being 46 × 80 × 65 Å. We have also calculated a 20 Å resolution three-dimensional (3D) map of the microtubule by cryoelectron microscopy and helical reconstruction and established the map polarity by comparison with previous data (Sosa and Milligan, 1996; Sosa et al., 1997). The 3D map shows that the inside and outside microtubule surfaces are very distinctive. The outside surface is characterized by a shallow zigzag of density that forms the crest of the protofilament. In a side view, this surface is fairly flat with very shallow undulations. In contrast, the inside surface is deeply corrugated, with the connections between protofilaments lying close to the inner surface. Here we have docked the crystal structure of tubulin into the 3D map of the microtubule to create a near atomic model of the microtubule. The model shows the detailed architecture of the microtubule and provides insight into the molecular basis for the observed properties of microtubules.

Results

Microtubule Docking

As the high-resolution model was obtained from a polymerized form of tubulin (Nogales et al., 1998a), the structure of the complete protofilament is readily available from the electron crystallographic data. Thus, docking the high-resolution and low-resolution structures was greatly facilitated by fitting the protofilament as a unit. Fitting was carried out first manually by rotating the atomic model of the protofilament around its axis and by translating along the microtubule length. This procedure was repeated for both the up and down orientations of the protofilament. Only one orientation, rotation, and translation fit within the microtubule map, unambiguously defining the polarity and orientation of the protofilament atomic model (Figures 1B–1D). Subsequently, the fitting was quantitatively tested by computing a correlation between the microtubule reconstruction and a density map calculated from the atomic model at a resolution of 2 Å. As a function of rotation of the model about the protofilament axis, the correlation has a strong peak that defines the orientation of the model to within ~5° (Figure 1E). Such rotation would result in movement at the outer surface of the protofilament of less than 3 Å. The orientation obtained by this method is the same as that found by the visual docking. Similarly well-defined correlation peaks were found for translation along and perpendicular to the axis, defining the position to within ~3 Å (data not shown), although these other degrees of freedom would not affect the interaction between

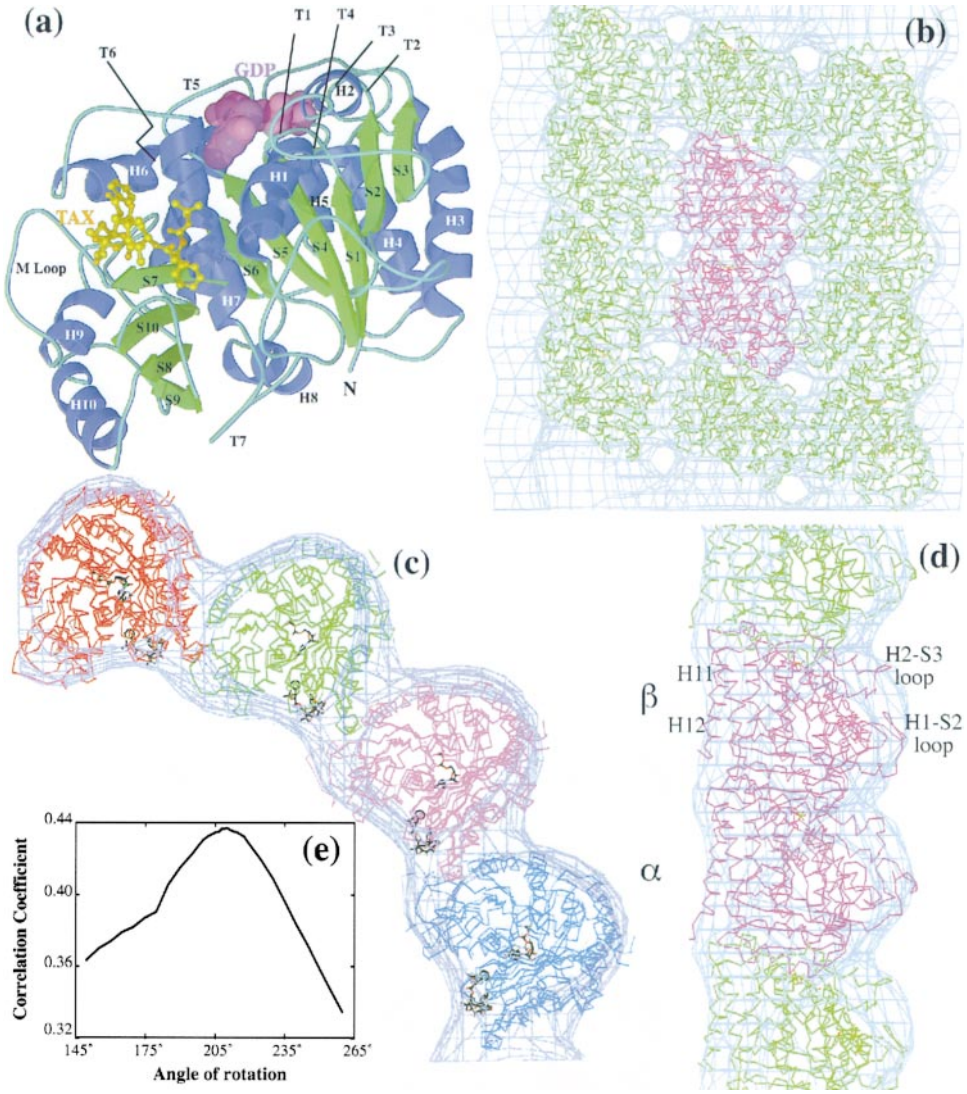

Figure 1. Docking of the Tubulin Crystal Structure into the Microtubule Map

(A) Electron crystallographic structure of β-tubulin from zinc-induced sheets stabilized with taxol. The different secondary structure elements as defined in Nogales et al. (1998a, 1998b) are indicated. Loops involved in nucleotide binding are labeled T1 to T7, where T7 interacts with the nucleotide of the next tubulin subunit down. The loop marked "M loop" is important in lateral interactions between protofilaments in the microtubule (see text). Figure generated with Raster 3D (Merrit and Murphy, 1994).

(B–E) Docking of the crystal structure of the tubulin protofilament from zinc sheets into the 20 Å 3D map of the microtubule. The microtubule map was obtained by helical reconstruction of ice-embedded microtubules with 15 protofilaments and a four-start helix as described in Sosa et al. (1997). (B) Front view of the docking shown from the outside of the microtubule with the plus end at the top. Three protofilaments, each with four tubulin monomers, are shown in green, except for the central dimer, which is shown in magenta. (C) Cross section of the microtubule docking showing four adjacent protofilaments in red, green, magenta, and blue, as seen from the plus end. Nucleotides and taxoid molecules are shown in black. (D) Lateral view of a single protofilament. The α and β subunits of the dimer in magenta are indicated, as well as the H1-S2 and H2-S3 loops on the inside surface of the microtubule and H11 and H12 on the outside of the microtubule. Figure generated with O (Jones et al., 1991). (E) Cross correlation between the microtubule density and a density map computed from the atomic model as a function of rotation around the protofilament axis. The correlation was calculated in real space using a program written as a module in AVS (Advanced Visual Systems, Inc.), allowing visualization of the relative positions of the two structures along with correlation calculation. The correlation coefficient was computed as:

$$C = \frac{\sum_1^N d_1 \cdot d_2 - \sum_1^N d_1 \cdot \sum_1^N d_2/N}{\sqrt{\left(\sum_1^N d_1^2 - \left(\sum_1^N d_1\right)^2/N\right) \cdot \left(\sum_1^N d_2^2 - \left(\sum_1^N d_2\right)^2/N\right)}}$$

where d_1 and d_2 are densities in the two structures, the sums are taken over all voxels in the map derived from the atomic model, and N is the number of voxels in the volume. The apparent low values for the coefficient are due to the difference in resolution between the model and the experimental map. When the model density was calculated to 20 Å, the best coefficient became close to 1 (data not shown).

protofilaments. When the model was tested with the polarity inverted, the best correlation was 0.40, well below the maximum obtained for the protofilament in the up orientation.

The External and Lumenal Microtubule Surfaces

The overall surface topography of the microtubule wall in the model follows closely the general features seen in low-resolution reconstructions. On the outside, there are deep grooves between protofilaments, and on the inside there are grooves following the "four-start" helix (Figures 1C and 1D) (the microtubules used for the reconstruction had 15 protofilaments and followed a four-start helix, which corresponds to the three-start of microtubules with 13 protofilaments [Sosa et al., 1997]). The intersection between the two sets of grooves between the protofilaments creates holes or fenestrations in the wall. These fenestrations were prominent features in negative stain reconstructions (Amos and Klug, 1974). The high-resolution model now brings these fenestrations into sharp focus and reveals them as open channels approximately 10 Å in diameter (Figures 1B and 5).

The outside surface of the microtubule is dominated by the C-terminal helices H11 and H12 and the well-defined loop between H10 and S9 (Figure 1D). These structural elements define a shallow zigzag path on the crest of each protofilament. The atomic model of tubulin lacks the last 18 C-terminal residues in β-tubulin and the last 10 residues in α-tubulin, which are disordered in the zinc sheets. As the high-resolution structure fits snugly within the 20 Å resolution microtubule map with no unoccupied space, it follows that these C-terminal regions are also disordered in microtubules assembled from purified tubulin. Completing the outside surface of the microtubule are, on one side of the crest, the H8-S7 loop, the C-terminal halves of H4 and H5, and the H11-H12 loop; on the other side are H10, the H9-S8 loop, and the last residues in loop T5.

In contrast to the outside surface of the microtubule, where long alpha helices are the predominant feature, the inside surface is dominated by the presence of long loops: the H1-S2 loop, the H2-S3 loop, and the S9-S10 loop (Figure 1D). This last loop, together with parts of H1, H6, H7, and S7 in β-tubulin, form the taxol-binding pocket in the high-resolution structure from zinc sheets (Nogales et al., 1998a) (see Figure 5).

Longitudinal Contacts in Protofilaments

The longitudinal interfaces between monomers and dimers (intradimer and interdimer interfaces, respectively) are very similar topologically and involve equivalent structural elements in α- and β-tubulin. We will focus first on the common attributes of these two contacts. The interfaces are very extensive, with a total surface of about 3000 Å^2 being buried upon formation of the dimer (Nogales et al., 1998b) or in a polymerization event. This interface shows an exquisite shape complementarity between monomers and a combination of hydrophobic and polar contacts (Figures 2 and 3 and Table 2). The structural elements interacting at this interface are indicated in Table 1.

Approximately 52% of the residues involved in the formation of the dimer are totally conserved within the α- and β-tubulin subfamilies, and about 40% of those at the dimer–dimer interface (data on conservation from Burns and Surridge, 1993). The most prominent interactions between residues of consecutive monomers are shown in Table 2. The nucleotide lies in the center of the interface and plays an important role in the interaction (Figure 2). Three major areas of longitudinal contacts between tubulin subunits are defined in Tables 1 and 2 and Figure 3. Zone A, toward the outside surface of the microtubule, involves the interaction of the H10-S9 loop in one monomer with H11 and loop T5 in the next monomer down. H10 also interacts with H6 and the H6-H7 loop of the previous monomer. Zone B includes the interaction of H8 with the N-terminal end of T5, with T3, and with a highly conserved region in the H11-H12 loop in the next monomer down. The last area, zone C, is close to the lumen of the microtubule and involves direct interaction of loop T7 with the nucleotide and adjacent regions of the previous monomer, T1, H2, and H7.

Residue differences between the intradimer and interdimer interfaces are indicated in Table 2. Some of those residues contribute to the interface via their main chain atoms. A cluster of significant side chain differences is present in zone C. Side chains involved directly in contacts at the intradimer interface, β:Q247, α:T225, α:T73, and α:G77 (Figure 3E), have disappeared or been shortened for the interdimer contact: α:G247, β:G225, β:G73, and β:S77 (Figure 3F). Two major differences are present in zone B. Residues β:R253 and α:D98 form a salt bridge at the intradimer interface (Figure 3C), which must contribute significantly to the energy of dimer formation (these residues are totally conserved in all known α- and β-tubulin sequences). The equivalent residues at the dimer–dimer interface are α:T253 and β:G98 (Figure 3D). The result of these differences is that the longitudinal interface toward the lumen of the microtubule is significantly weaker between dimers than between monomers within the dimer. Finally, an important additional difference is the residue at position 254. In β-tubulin, this residue is a lysine that sits very close to the γ-phosphate at the N site (Figure 3C). In α-tubulin, the residue is a glutamate that has been proposed to catalyze polymerization-driven hydrolysis at the E site (Nogales et al., 1998b), based both on the position of the residue in the tubulin atomic model (Figure 3D) and on mutagenesis studies of the equivalent residue in FtsZ (Dai et al., 1994). Alanine scan mutations in yeast β-tubulin have shown D251A-R253A-K254A to be a lethal mutation (Reijo et al., 1994).

Lateral Contacts between Protofilaments

Docking the high-resolution model of the protofilament into the microtubule map places a number of structural elements on the sides of the protofilaments in close proximity to each other. These elements lie at low microtubule radius and occupy the connections between protofilaments seen in the lower-resolution 3D maps (Figure 1C). The level of certainty in the fitting regarding rotation of the protofilaments (±5°) is more than sufficient to clearly identify the structural elements that are involved in the protofilament interactions in the microtubule (Table 1). Determination of the precise residues involved

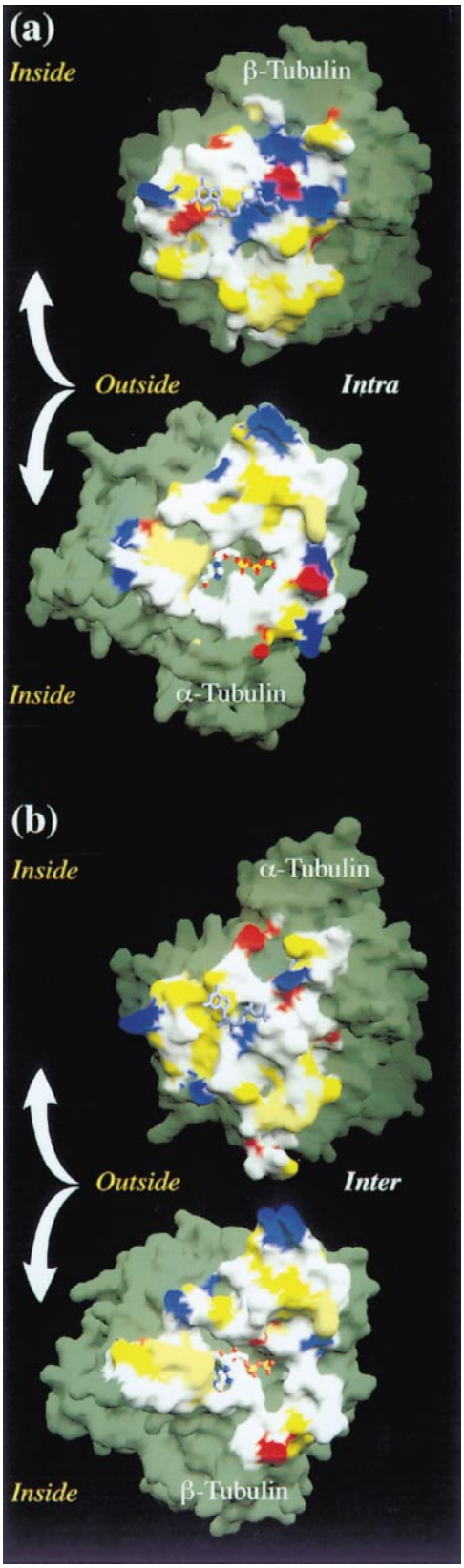

Figure 2. Longitudinal Interfaces along Protofilaments

Longitudinal contact interfaces (A) between monomers within the dimer and (B) between dimers. Surfaces involved in subunit contacts were defined as those 4 Å or less from the next subunit. The two subunits were rotated away from each other by 90° around the horizontal axis to allow visualization of the interface. Nucleotides are shown colored in the monomers where they are bound and are shown also in gray above the other monomer for easier reference. The interacting surfaces are colored according to the character of the residues underneath: blue for positively charged residues (Lys, Arg), red for negatively charged (Asp, Glu), white for polar (Ser, Thr, Cys, Asn, Gln, His, Gly), yellow for hydrophobic (Ala, Val, Leu, Ile, Met, Phe, Pro), and pale yellow for Trp and Tyr. Both polar and hydrophobic interactions contribute to the intradimer and interdimer interfaces, with the intradimer having a small electrostatic component. The contacts are extensive and highly complementary in shape so that van der Waals interactions are important. Figure generated with GRASP (Nicholls, 1993).

Table 1. Interacting Elements in Tubulin Subunits

Longitudinal Contacts

H10	Zone A	H6, H6-H7
H10-S9		H11
S9		H11-H12
	Zone B	T5
H8		T3
H3-S4		γ-Phosphate
	Zone C	Phosphates
T7		T2 (?)
		T1
		Guanine, F224

Lateral Contacts

H10 (323,338)	H4-S5 (160-163)
H9, H9-S8 (289-300)	H3 (113-129)
H6, H6-H7 (214-218)	S3 (94?)
S7-H9 (279-287)	H2-S3 (88-91)
	H1-S1 (51-55 ??)

Interactions between secondary structure elements of tubulin at longitudinal and lateral interfaces. Three main zones of interactions, A, B, and C, can be recognized at the longitudinal interface (see Table 2 for an account of the residues directly involved in this interaction). For lateral interactions, the sections of the sequence most likely to be involved in the contact are indicated in parentheses.

in lateral interactions would not be meaningful, because the different interprotofilament geometry in zinc sheets and microtubules strongly suggests some local conformational changes in the regions of interaction, particularly concerning loops.

Compared to the longitudinal contacts, lateral interaction surfaces show a marked electrostatic character (Figure 4). The S7-H9 loop appears to be the central element of the interaction (Table 1 and Figure 5). We refer to this loop as the M loop (for microtubule loop). It projects out from one side of the protofilament and makes close contacts with H3, the C-terminal part of the H2-S3 loop, and part of the H1-S2 loop in the adjacent protofilament (Figure 5). Three additional regions lie very

Table 2. Longitudinal Interactions

α-Tubulin	INTERDIMER	β-Tubulin
β-Tubulin	*INTRADIMER*	*α-Tubulin*
V324, P325, K326		T221, P222, T223, Y224
S M K		*R P T Y*
N329		K176, E207, Y210 (?)
D		*Q E Y*
W346, C347, P348		F404, M398, E183, T180
W I P		*F M E A*
A333, T349		K176, V177
L N		*Q V*
Zone A		
T253		G98, A99, G100,
R — *Salt Bridge* —		*D A G*
E254 — Hydrolysis Catalyst —		N101, γ Phosphate
K		*N γ Phosphate*
Q256, T257, V260, P261		F404, W407
A V V P		*F W*
N258		D179, T180
N		*T A*
F262		A403, H406
Y		*A H*
G131, Q133		G95, Q96, S97, G98
G C		*G K E D*
Zone B		
A247, L248		Y224, T225, Guanosine
Q L		*Y G Guanosine*
N249		Q11, T73, E77, Phosphates
N		*Q G S Phosphates*
D251		Phosphates
D		*Phosphates*
Zone C		

Residues involved in longitudinal interaction between tubulin subunits. The residues on the left column interact with those in the right column (numbering of residues refers to the aligned sequences of α- and β-tubulin and includes gaps in β-tubulin [Nogales et al., 1998]). Residues involved in intradimer interactions are shown in italics and those involved in contacts between dimers are shown in roman characters. Boxes indicate residues that are different at the intra- and interdimer interfaces.

close to the lateral interfaces between protofilaments: H9 and part of the following loop; the C-terminal end of H6 and the following loop, which are likely to make contact with H3 and S3 in the adjacent molecule; and H10, which is within contact distance of the C-terminal ends of H3 and H4.

It is generally established that a B lattice is the predominant arrangement of tubulin monomers in the microtubule lattice (Song and Mandelkow, 1993), where lateral contacts are made between homologous subunits, that is, α–α, β–β. Table 2 shows the segments on the tubulin sequences broadly involved in lateral contacts. Although equivalent structural elements contribute to the α–α and β–β lateral interfaces, the residues involved in each case are significantly different. The central element for lateral interactions, the M loop, includes a segment of the sequence that is one of the most divergent between α- and β-tubulin: α:AEKAYHEQ versus β:RGSQQYRA. Some important differences between α- and β-tubulin are also present on the other side of the interface (H3, loops H1-S2 and H2-S3, S3, and H4), in particular a two-residue insertion in α-tubulin within the H1-S2 loop. These sequence differences between the α and β subunits are at the heart of the definition of the microtubule lattice, that is, the preference between homologous (B lattice) and heterologous (A lattice/seam) lateral contacts.

Discussion

Microtubule Docking

The excellent fit of the atomic model of tubulin from zinc-induced sheets into the microtubule reconstruction strongly indicates that the conformation of the protofilament is highly conserved for the two polymers, with no major change in the structure of tubulin or in the longitudinal contacts between subunits. Differences between the two polymers should therefore be restricted to local changes at the sites of lateral interactions.

The detailed complementarity in the shape of the microtubule map and the crystal structure of the protofilament made the visual docking straightforward. Calculation of the correlation between the two structures confirms the manual fit and gives a quantitative measure of the precision of the docking. The correlation plots indicate that the rotation is very highly constrained to within five degrees, corresponding to less than 3 Å movement at the molecular surface. This level of uncertainty, which is of the same order of that for translation and radial displacement, does not affect the identification of the structural elements involved in lateral contacts between tubulin subunits.

In previous reports, the tubulin dimer was defined based on the position of the hydrolyzed (exchangeable) and nonhydrolyzed (nonexchangeable) nucleotides, the observation that one interface—likely the intradimer interface—is tighter, and the localization of residues involved in colchicine binding at the intradimer interface (Nogales et al., 1998a). Thus, the identification of the dimer, together with the unique and unambiguous fit of the protofilament model into a microtubule map of known polarity (Sosa et al., 1997), allows us to definitively establish the identity of the monomer at the microtubule ends; β-tubulin crowns the plus end of the microtubule and α-tubulin crowns the minus end. This result agrees with EM observations of the ends of microtubules decorated with kinesin (Hirose et al., 1995a) and the immunolabeling of minus ends by an anti-α-tubulin antibody (Fan et al., 1996).

The External and Lumenal Microtubule Surfaces

As the high-resolution structure of the protofilament fits snugly within the microtubule map, without unoccupied space, the C-terminal regions must also be disordered in microtubules assembled from purified tubulin. This conclusion is in agreement with previous experimental data (Sackett, 1995; Chau et al., 1998). The C-terminal regions, although not resolved in the high-resolution structure, must be located on the outside of the microtubule following helix H12. This location is also suggested by their accessibility to proteases, antibodies, and their role in binding MAPs (Ludueña et al., 1992; Andreu, 1993;

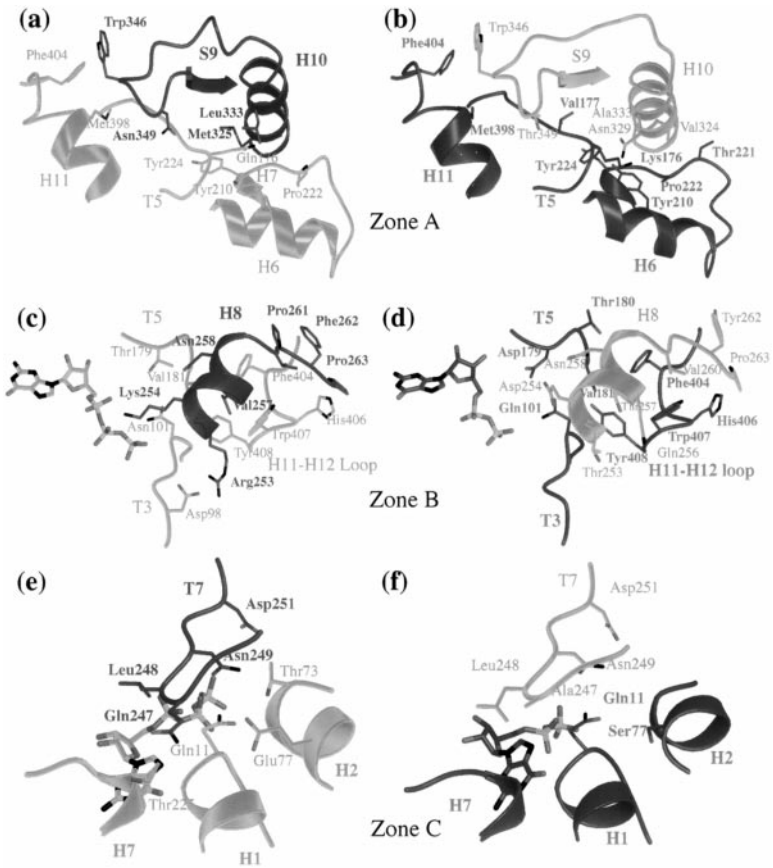

Figure 3. Structure of the Longitudinal Contacts

Longitudinal contacts between α-tubulin (light gray) and β-tubulin (dark gray) at the intradimer interface (A, C, E) and at the interdimer interface (B, D, F). The side chains for some of the residues involved are shown. Figure generated with Raster 3D (Merrit and Murphy, 1994).

Sackett, 1995). The outside surface of the microtubule is therefore characterized by the presence of both well-ordered (H11, H12, loop H10-S9) and disordered regions (C-terminal residues). These regions form the crest of the protofilament to which motors have been shown to bind (Hirose et al., 1995b; Hoenger et al., 1995; Kikkawa et al., 1995; Arnal et al., 1996; Sosa and Milligan, 1996). It is noteworthy that yeast β-tubulin mutations of the charged residues in H12 are lethal (Reijo et al., 1994), most likely due to the disruption of motor–microtubule interactions.

In the model, taxol lies on the inside surface of the microtubule, near lateral contacts between protofilaments (Figure 5). In fact, the taxane ring of taxol sits at the N-terminal end of the M loop, which is essential for lateral interactions both in zinc sheets (Nogales et al., 1998a) and microtubules. Experimental results from other groups provide strong support for a common binding site of taxol in tubulin, for both microtubules and zinc sheets. For example, the taxol-binding elements that have been identified by photocross-linking studies in microtubules (Rao et al., 1994, 1995) lie in close proximity to taxol in the crystallographic model (Nogales et al., 1998a). Furthermore, mutations affecting taxol cytotoxicity in ovarian cancer cells (Giannakakou et al., 1997) map to the S9-S10 loop that defines part of the taxol pocket and to a phenylalanine in S7 whose side chain is stacked against the C3′ phenyl group of taxol. Recent results on the rapid appearance of fluorescence in assembled microtubules upon addition of labeled taxol were interpreted to mean that the binding site was on the outside surface of the microtubule, as diffusion from the open microtubule ends could not account for the rapid kinetics of labeling (Evangelio et al., 1998). However, our model suggests that rapid luminal access could occur via the fenestrations in the microtubule wall (see Figure 5) or via defects in the microtubule lattice (Chrétien et al., 1992).

The position of α:Lys40 (within the H1-S2 loop) on the inside surface of the microtubule seems somehow difficult to reconcile with its susceptibility to proteases (de Pereda and Andreu, 1996) and acetylation in assembled microtubules (Maruta et al., 1986). However, data indicate that acetylation is a slow process compared to microtubule assembly (Piperno et al., 1987) and that it occurs from the ends of the microtubule (Wilson and Forer, 1997), suggesting a slow diffusion of the acetyltransferase down the microtubule lumen. Furthermore, immunoelectron microscopy experiments using antibodies specific for acetylated tubulin show that in conditions that preserve the integrity of the microtubule wall, label is only present at the end of microtubules or in positions where the microtubule is broken, indicating that the large antibodies could not reach the acetylated site on the inside of the microtubule (J. Rosenbaum and K. Johnson, personal communication). Together with

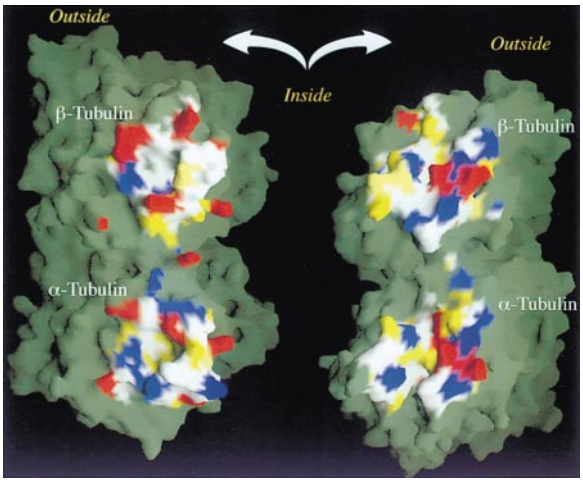

Figure 4. Lateral Interfaces between Protofilaments

Lateral contact interfaces. Surfaces involved in subunit contacts were defined as those 5 Å or less from the next subunit. This distance was chosen because of the uncertainty in the conformation of the structural elements involved (see text). The contact surface of interaction should therefore be an overestimation. The two subunits have been rotated away from each other by 90° around the vertical axis. The interacting surfaces are colored according to the character of the residues underneath, as indicated in Figure 3. The contacts show an important electrostatic component. Figure generated with GRASP (Nicholls, 1993).

our model, these data suggest that the acetyltransferase and the proteases diffuse slowly along the ~150 Å diameter lumen of the microtubule.

Contacts in and between Protofilaments

The longitudinal interactions between tubulin subunits along a protofilament are well determined from the crystal structure of tubulin zinc sheets. The quality of the fitting supports the idea that the conformation of the tubulin dimer and the interaction between subunits along the protofilament are extremely similar in zinc sheets and microtubules. Comparison of intra- and interdimer contacts show that the longitudinal interactions are stronger and more extensive between monomers within the dimer than at the dimer–dimer interfaces, particularly near the lumen of the microtubule. This observation suggests that the loss of the γ-phosphate at the E site, which is directly involved in contact between dimers, should further weaken the interaction between dimers at lower radius, promoting the outward curling of the protofilament and its consequent disassembly, as observed by cryoelectron microscopy (Mandelkow et al., 1991).

The accuracy of the docking allows us to identify the structural elements in tubulin involved in lateral interactions. Identification of the precise residues is not possible, not only because the present docking has a certainty of about 3 Å (corresponding to 5° of rotation), but also because the elements involved in the contact are expected to change conformation, to a certain extent, in the presence of zinc. That conformational change, related to the antiparallel arrangement of protofilaments in the sheets, is most likely confined to the structure of the M loop and the precise orientation of helix H3. In addition, the H1-S2 and the H2-S3 loops, which are very poorly ordered in the high-resolution structure obtained from zinc sheets, should adopt a defined conformation in the microtubule as they become involved in the interactions between protofilaments.

The position of the tubulin interfaces in the microtubule agrees very well with the protection of four proteolytic sites in tubulin upon microtubule polymerization (de Pereda and Andreu, 1996). One of these sites is the main trypsin digestion site in α-tubulin at Arg-339 (Brown and Erickson, 1983; Mandelkow et al., 1985; Sackett and Wolff, 1986; de Pereda and Andreu, 1996). This residue is near the lateral interaction between helix H10 in one monomer and helices H3 and H4 in the adjacent subunit. A second polymerization-protected site in α-tubulin is at the nicking point by endoproteinase Lys-C, Lys-280, which in our model is within the main lateral interface at the M loop (de Pereda and Andreu, 1996). Similar protection upon polymerization occurs for the main chymotrypsin site in β-tubulin at Tyr-283 (Brown and Erickson, 1983; Mandelkow et al., 1985; Sackett and Wolff, 1986; de Pereda and Andreu, 1996). Finally, the β-tubulin cleavage by clostripain at Arg-123 that is totally abolished in microtubules (de Pereda and Andreu, 1996) is located in H3.

Interestingly, temperature-sensitive alanine scan mutants in yeast, both for β-tubulin (Reijo et al., 1994) and α-tubulin (K. Richards et al., in preparation), map to polymerization interfaces. In β-tubulin, the temperature-sensitive mutants map mainly to H3, the M loop, and the H1-S2 loop, the most important regions for lateral contacts, as well as H10 and loops T6, T5, and H11-H12, regions directly involved in longitudinal contacts (H10 at the intradimer contact, and loops T6, T5, and H11-H12 at the interdimer interface). In addition, some lethal mutations in yeast β-tubulin are close to or at the interface involved in the formation of the dimer, namely those in T7 and H8 (also involved in nucleotide binding), H10, and loop H10-S9 (Reijo et al., 1994).

Microtubules are polymorphic both in vivo and in vitro, being constructed from as few as 9 or as many as 18 protofilaments (Chrétien and Wade, 1991). There is thus considerable flexibility in the interprotofilament contacts that must be capable of accommodating different angles between adjacent protofilaments (~20°–40° from planar). In this context, the N- and C-terminal parts of the M loop seem to be well placed to function as a hinge. They position the middle part of the loop away from the tubulin surface and could allow it to swing azimuthally. H3 is similarly articulated, though perhaps not to the same extent, by loops at each end of the helix. Thus, parts of the polypeptide chain before and after the interacting regions of the M loop and H3 could provide flexibility without compromising the interactions between these structural elements.

Nucleotide Hydrolysis and Dynamic Instability

As described before, the docking, together with the definition of the dimer, leads to the conclusion that the plus

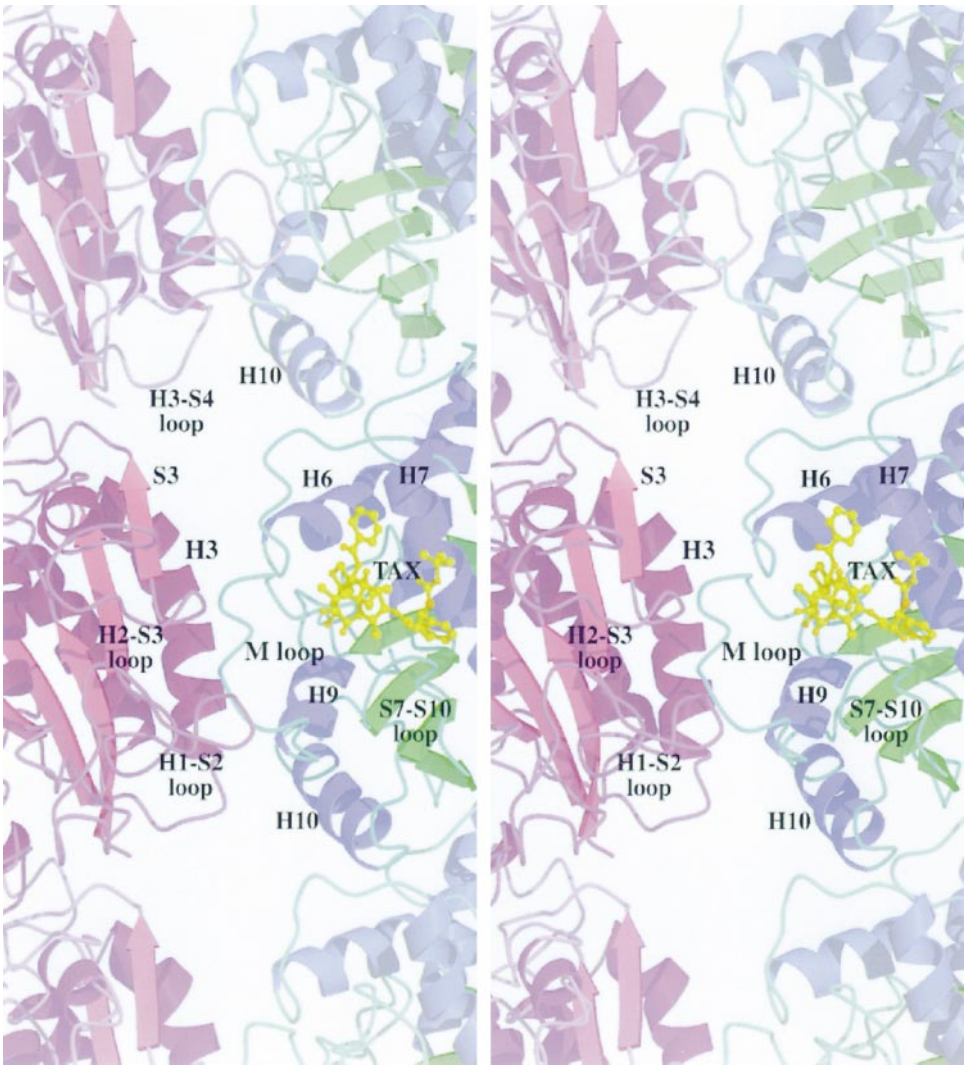

Figure 5. Structure of the Lateral Contacts

Stereo image of the lateral interaction between tubulin subunits. β-tubulins are shown in the center area, while α-tubulins (lighter tones) are above and below. Secondary structure elements involved in the contact, in binding taxol (taxotere in the crystallographic model), or in defining the fenestrations between protofilaments are indicated. Figure generated with Raster 3D (Merrit and Murphy, 1994).

end of the microtubule is crowned by β subunits and the minus end by α subunits (Figure 1). Furthermore, given the positions of the nucleotides at the interfaces between subunits, the nucleotide at the E site in the last dimer faces the solvent at the plus end, explaining the nucleotide exchange observed to occur at plus ends (Mitchison, 1993). Upon arrival of a new dimer at the plus end, residues in loop T7 and helix H8 in α-tubulin of the incoming dimer interact with the nucleotide of the receiving β subunit (Nogales et al., 1998b). This nucleotide is consequently hydrolyzed, and the resulting GDP becomes buried in the interface and therefore nonexchangeable. As GTP in the newly added dimer is unaffected by polymerization, the plus end should have a layer of GTP subunits.

The situation at the minus end is different. The receiving minus end is formed by the surface of α-tubulin containing the catalytic residue, and it is the E site nucleotide of the incoming dimer that is hydrolyzed following a new polymerization event. This means that, except under conditions where hydrolysis and/or P_i release is slow compared to subunit addition (i.e., high concentration of free GTP-tubulin), no GTP cap should exist at the minus end.

The involvement of the nucleotide in longitudinal contacts and the central role of H3 in lateral interactions are of special relevance for dynamic instability. T3, the loop preceding H3, is directly involved in binding the γ-phosphate and should be particularly sensitive to hydrolysis of the E site nucleotide (Nogales et al., 1998b). In that respect, and in spite of the established differences between tubulins and the classical GTPases (Nogales et al., 1998b), loops T3 and H3 can be considered the equivalent of the Switch II region. We postulated above how the loss of the γ-phosphate should weaken the dimer–dimer interface, inducing the curling and subsequent disassembly of the protofilament. Lateral interactions should also be affected by nucleotide hydrolysis

through H3. Hydrolysis could induce a conformational change in H3 transmitted directly through T3, resulting in weakening of the contacts between adjacent protofilaments. It is not difficult, therefore, to imagine that the presence of the γ-phosphate is required to maintain strong lateral interactions and that these interactions at the capped ends could be enough to stabilize the structure of the whole polymer.

The stability of a microtubule end could be determined mainly by the lateral interactions at the very last monomer, with the second monomer in the dimer having a smaller additional effect. The effect of hydrolysis on lateral contacts should be limited mostly to the β subunit, establishing further differences between the plus and minus ends. The last lateral contact at the minus end is always made by an α subunit and should be basically the same, independent of the nucleotide state. Thus, the minus end will be fairly stable with respect to lateral interactions (even in the absence of a GTP cap), with a strong "terminal" contact between α subunits. In contrast, the plus end will be in one of two very different states concerning lateral interactions, depending on whether the contacts at the very last monomer are between β subunits containing GTP (strong contacts) or GDP (weak contacts). The very different dynamic behaviors observed at the plus and minus ends of microtubules (Walker et al., 1989) therefore result from the fact that tubulin is a dimer where only one monomer is regulated by nucleotide hydrolysis.

In summary, the minus end should generally lack a GTP cap, but will end on laterally interacting α-tubulins. The plus end should generally have a monolayer GTP cap, but the loss of this cap (by nucleotide exchange, dissociation of end dimers, or addition of GDP subunits) will produce an end of β-tubulins containing GDP that interact weakly laterally. This model is in agreement with a more dynamic plus end, with fast growth and shrinkage states and frequent catastrophes and rescues, while the minus end will be less dynamic, with infrequent rescues and catastrophes, and will be generally shrinking at a lower rate. The structural basis for this model should serve to extend statistical models aimed at reproducing dynamic instability (Martin et al., 1993).

In this context, the action of taxol could be understood as a strengthening of the lateral contacts between β subunits that "overrides" the hydrolysis-induced conformational change in H3 by affecting the M loop at the other side of the interface (different or additional effects of taxol involving an allosteric effect far from its binding site—for example, stabilization of longitudinal contacts, or a change in the shape of the dimer as a whole—seem less likely but cannot yet be disregarded). In agreement with experimental data (Derry et al., 1998), our model indicates that the stabilizing action of taxol should be more effective at the plus end, which is crowned by β-tubulins. The position of taxol on the β subunit is occupied in the α subunit by the extra eight amino acids inserted in the S9-S10 loop, which is by the M loop. Taxol could, therefore, act by mimicking the stabilizing effect that the extra residues in α-tubulin have on the M loop. An interesting possibility to be considered is that small endogenous molecules in the cell could also bind to this site in β-tubulin, or that small peptides could be designed to stabilize microtubules in a taxol-like fashion.

Conclusions

Our model of the microtubule establishes the position of the different structural elements in tubulin with respect to the inside and outside and plus and minus ends of the microtubule. It identifies the regions in the tubulin sequence involved in longitudinal and lateral interactions and provides insight into the differences between intradimer and interdimer interactions and between A and B lattices. The model allows us to link the processes of polymerization and hydrolysis and provides insight into the effect of hydrolysis on the depolymerization of microtubules and on the stabilizing effect of taxol. Finally, the model correlates the different dynamic behaviors of the plus and minus ends with the fact that only one monomer in the tubulin heterodimer is regulated by its nucleotide state.

Experimental Procedures

The crystal structure of tubulin at 3.7 Å resolution was obtained from zinc-induced two-dimensional crystalline sheets of tubulin, stabilized by taxol, and studied by electron crystallography (Nogales et al., 1998a). Details on crystal growth and electron crystallographic procedures can be found in Nogales et al. (1997, 1998a). The 20 Å resolution density map for the microtubule was obtained by cryo-electron microscopy of frozen-hydrated microtubules and image analysis using helical reconstruction procedures (Sosa et al., 1997). Microtubules with 15 protofilaments and a four-start helix, having a true helical arrangement of tubulin monomers, were selected for analysis.

Docking of the crystal structure of the protofilament into the microtubule reconstruction was done both visually, using the crystallographic program "O," and by a maximization procedure of the correlation coefficient between the microtubule density map and a density map generated from the atomic coordinates of the protofilament. For more details, refer to the text and the legend to Figure 1.

Acknowledgments

This work was supported by NIH grants GM46033 (K. H. D.), GM51487 (E. N. and K. H. D.), GM52468 (R. A. M.), and by the Office of Basic Energy Sciences of the U.S. Department of Energy under contract number DE-AC03-76SF00098 (E. N. and K. H. D.).

Received August 13, 1998; revised December 9, 1998.

References

Amos, L.A., and Klug, A. (1974). Arrangement of subunits in flagellar microtubules. J. Cell Sci. *14*, 523–549.

Amos, L.A., and Baker, T.S. (1979). The three-dimensional structure of tubulin protofilaments. Nature *279*, 607–612.

Andreu, J.M. (1993). Site-directed antibodies to tubulin. Cell Motil. Cytoskeleton *26*, 1–6.

Arnal, I., Metoz, F., DeBonis, S., and Wade, R.H. (1996). Three-dimensional structure of functional motor proteins on microtubules. Curr. Biol. *6*, 1265–1270.

Brown, H.R., and Erickson, H.P. (1983). Assembly of proteolytically cleaved tubulin. Arch. Biochem. Biophys. *220*, 46–51.

Burns, R.G., and Surridge, C.D. (1993). Tubulin: conservation and structure. In Microtubules, J.S. Hyams and C.W. Lloyd, eds. (New York: John Wiley and Sons, Inc.), pp. 3 and 32.

Chau, M.-F., Radeke, M.J., Barasoain, I., de Ines, C., Kohlstaedt, L.A., and Feinstein, S.C. (1998). The microtubule associated protein

tau cross-links to two distinct sites on each α and β tubulin monomer via separate domains. Biochemistry, in press.

Chrétien, D., and Wade, R.H. (1991). New data on the microtubule surface lattice. Biol. Cell *71*, 161–174.

Chrétien, D., Metoz, F., Verde, F., Karsenti, E., and Wade, R.H. (1992). Lattice defects in microtubules: protofilament numbers vary within individual microtubules. J. Cell Biol. *117*, 1031–1040.

Dai, K., Mukherjee, A., Xu, Y., and Lutkenhaus, J. (1994). Mutations in FtsZ that confer resistance to SulA affect the interaction of FtsZ with GTP. J. Bacteriol. *175*, 130–136.

de Pereda, J.M., and Andreu, J.M. (1996). Mapping surface sequences of the tubulin dimer and taxol-induced microtubules with limited proteolysis. Biochemistry *35*, 14184–14202.

Derry, W.B., Wilson, L., and Jordan, M.A. (1998). Low potency of taxol at microtubule minus ends: implications for its antimitotic and therapeutic mechanism. Cancer Res. *58*, 1177–1184.

Evangelio, J.A., Abal, M., Barasoain, I., Souto, A.A., Lillo, M.P., Acuna, A.U., Amat-Guerri, F., and Andreu, J.M. (1998). Fluorescent taxoids as probes of the microtubule cytoskeleton. Cell Motil. Cytoskel. *39*, 73–90.

Fan, J., Griffiths, A.D., Lockhart, A., Cross, R.A., and Amos, L.A. (1996). Microtubule minus ends can be labelled with a phage display antibody specific to α-tubulin. J. Mol. Biol. *259*, 325–330.

Giannakakou, P., Sackett, D.L., Kang, Y.K., Zhan, Z., Buters, J.T., Fojo, T., and Poruchynsky, M.S. (1997). Paclitaxel-resistant human ovarian cancer cells have mutant beta-tubulins that exhibit impaired paclitaxel-driven polymerization. J. Biol. Chem. *227*, 17118–17125.

Hirose, K., Fan, J., and Amos, L.A. (1995a). Re-examination of the polarity of microtubules and sheets decorated with kinesin motor domain. J. Mol. Biol. *251*, 329–333.

Hirose, K., Lockhart, A., Cross, R.A., and Amos, L.A. (1995b). Nucleotide-dependent angular change in kinesin motor domain bound to tubulin. Nature *376*, 277–279.

Hoenger, A., Sablin, E.P., Vale, R.D., Fletterick, R.J., and Milligan, R.A. (1995). Three-dimensional structure of a tubulin-motor-protein complex. Nature *376*, 271–274.

Jones, T.A., Zou, J.-Y., Cowan, S.W., and Kjelgaard, M. (1991). Improved methods of building protein models in electron density maps and the location of errors in these models. Acta Crystallogr. A *47*, 110–119.

Kikkawa, M., Ishikawa, T., Wakabayashi, T., and Hirokawa, N. (1995). Three-dimensional structure of the kinesin head-microtubule complex. Nature *376*, 274–277.

Ludueña, R.F., Banerjee, A., and Khan, I.A. (1992). Tubulin structure and biochemistry. Curr. Opin. Cell Biol. *4*, 53–57.

Mandelkow, E.-M., Herrmann, M., and Rühl, U. (1985). Tubulin domains probed by limited proteolysis and subunit-specific antibodies. J. Mol. Biol. *185*, 311–327.

Mandelkow, E.-M., Mandelkow, E., and Milligan, R.A. (1991). Microtubules dynamics and microtubules caps: a time-resolved cryo-electron microscopy study. J. Cell Biol. *114*, 977–991.

Martin, S.R., Schilstra, M.J., and Bayley, P.M. (1993). Dynamic instability of microtubules: Monte Carlo simulation and application to different types of microtubule lattice. Biophys. J. *65*, 578–596.

Maruta, H., Greer, K., and Rosenbaum, J.L. (1986). The acetylation of alpha-tubulin and its relationship to the assembly and disassembly of microtubules. J. Cell Biol. *103*, 571–579.

Merrit, E.A., and Murphy, M.E.P. (1994). Raster3D version 2.0—a program for photorealistic molecular graphics. Acta Crystallogr. D *50*, 869–873.

Mitchison, T.J. (1993). Localization of an exchangeable GTP binding site at the plus end of microtubules. Science *261*, 1044–1047.

Nicholls, A. (1993). GRASP: Graphical Representation and Analysis of Surface Properties. (New York: Columbia University).

Nogales, E., Wolf, S.G., and Downing, K.H. (1997). Visualizing the secondary structure of tubulin: three-dimensional map at 4 Å. J. Struct. Biol. *118*, 119–127.

Nogales, E., Wolf, S.G., and Downing, K.H. (1998a). Structure of the αβ tubulin dimer by electron crystallography. Nature *391*, 199–203.

Nogales, E., Downing, K.H., Amos, L.A., and Lŏwe, J. (1998b). Tubulin and FtsZ form a distinct family of GTPases. Nat. Struct. Biol. *5*, 451–458.

Piperno, G., LeDizet, M., and Chang, X.-J. (1987). Microtubules containing acetylated a-tubulin in mammalian cells in culture. J. Cell Biol. *104*, 289–302.

Rao, S., Krauss, N.E., Heerding, J.M., Orr, G.A., and Horwitz, S.B. (1994). 3′-(p-Azidobenzamido)taxol photolabels the N-terminal 31 amino acids of β-tubulin. J. Biol. Chem. *269*, 3132–3134.

Rao, S., Orr, G.A., Chaudhary, A.G., Kingston, D.G.I., and Horwitz, S.B. (1995). Characterization of the taxol binding site on the microtubule. J. Biol. Chem. *270*, 20235–20238.

Reijo, R.A., Cooper, E.M., Beagle, G.J., and Huffaker, T.C. (1994). Systematic mutational analysis of the yeast beta-tubulin gene. Mol. Biol. Cell *5*, 29–43.

Sackett, D.L. (1995). Structure and function in the tubulin dimer and the role of the acidic carboxyl terminus. In Proteins: Structure, Function, and Engineering, B.B. Biswas and S. Roy, eds. (New York: Plenun Press), pp. 255–302.

Sackett, D.L., and Wolff, J. (1986). Proteolysis of tubulin and the substructure of the tubulin dimer. J. Biol. Chem. *261*, 9070–9076.

Song, Y.-H., and Mandelkow, E. (1993). Recombinant kinesin motor domain binds to β-tubulin and decorates microtubules with a B surface lattice. Proc. Natl. Acad. Sci. USA *99*, 1671–1675.

Sosa, H., and Milligan, R.A. (1996). Three-dimensional structure of ncd-decorated microtubules obtained by a back-projection method. J. Mol. Biol. *260*, 743–755.

Sosa, H., Dias, D.P., Hoenger, A., Whittaker, M., Wilson-Kubalek, E., Sablin, E., Fletterick, R.J., Vale, R.D., and Milligan, R.A. (1997). A model for the microtubule-Ncd motor protein complex obtained by cryo-electron microscopy and image analysis. Cell *90*, 217–224.

Walker, R.A., Inoue, S., and Salmon, E.D. (1989). Asymmetric behavior of severed microtubule ends after ultraviolet-microbeam irradiation of individual microtubules in vitro. J. Cell Biol. *108*, 931–937.

Wilson, P.J., and Forer, A. (1997). Effects of nanomolar taxol on crane-fly spermatocyte spindles indicate that acetylation of kinetochore microtubules can be used as a marker of poleward tubulin flux. Cell Motil. Cytoskeleton *37*, 20–32.